Laser and Particle Beams (2004), *22*, 289–300. Printed in the USA.

DOI: 10.1017/S0263034604223138

Easy spectrally tunable highly efficient X-ray backlighting schemes based on spherically bent crystals

T. PIKUZ,[1] A. FAENOV,[1] I. SKOBELEV,[1] A. MAGUNOV,[1] L. LABATE,[2] L.A. GIZZI,[2] M. GALIMBERTI,[2] A. ZIGLER,[3] G. BALDACCHINI,[4] F. FLORA,[4] S. BOLLANTI,[4] P. DI LAZZARO,[4] D. MURRA,[4] G. TOMASSETTI,[5] A. RITUCCI,[5] A. REALE,[5] L. REALE,[5] M. FRANCUCCI,[6] S. MARTELLUCI,[6] AND G. PETROCELLI,[6]

[1]Multicharged Ions Spectra Data Center of National Research Institute of Physical Technical and Radiotechnical Measurements Mendeleyev, Moscow, Russia
[2]Intense Laser Irradiation Laboratory, Istituto per i Processi Chimico-Fsisici, Consiglio Nazionale delle Recherché, Area della Ricerca di Pisa, Pisa, Italy
[3]Racah Institute of Physics, The Hebrew University of Jerusalem, Jerusalem, Israel
[4]Ente per le nuove technologie l'energia e l'ambiente, Unita' Technico Scientifica Tecnologie Fisiche Avanzate, C.R. Frascati, Rome, Italy
[5]Istituto Nazionale per la Fisica della Materia, Dipartamento di Fisica dell'Aquila and Laboratory Nazionale del Gran Sasso, Istituto Nazionale di Fisica Nucleare, Assergi, Italy
[6]Istituto Nazionale per la Fisica della Materia, Universitó di Roma Tor Vergata, Roma, Italy

(RECEIVED 1 November 2003; ACCEPTED 30 June 2004)

Abstract

New easy spectrally tunable backlighting schemes based on a spherically bent crystal are considered. Contrary to traditional backlighting scheme, in which the investigated objects should be placed between the backlighter and the crystal, for the considered schemes an object is placed downstream of the crystal, before the tangential or after the sagittal focus and an image of the object is recorded at the distance from the object corresponding to the needed magnification. The magnification is defined by the ratio of the distances from the sagittal focus to the detector and from the object to the sagittal focus. A ray-tracing modeling and experimental images of test meshes, obtained at incidence angles of the backlighter radiation of 10° and 22°, are presented. It is demonstrated that a simple linear transformation of the obtained astigmatic images allows reconstructing them as a stigmatic with an accuracy of 5–15%. For the spectral range around 9 Å a spatial resolution about 10 μm in a field of view of some square millimeters is achieved experimentally and confirmed by ray-tracing simulations.

Keywords: Plasma diagnostics; X-ray backlighting; X-ray imaging; X-ray optics

1. INTRODUCTION

Experiments on using spherically bent crystals for X-ray backlighting imaging of plasma objects were started practically 30 years ago (Belyaev *et al.*, 1976) and nowadays they are more and more widely applied for diagnostics of different plasma facilities (Pikuz *et al.*, 1995*a*, 1995*b*, 1997; Aglitskiy *et al.*, 1996, 1997, 1998, 1999, 2001*a*, 2001*b*; Brown *et al.*, 1997; Sanchez del Rio *et al.*, 1997, 1999; Holzer *et al.*, 1998; Koch *et al.*, 1998, 1999, 2003; Workman *et al.*, 1999, 2001; Sinars *et al.*, 2003*a*, 2003*b*). Despite of the fact that imaging of plasmas by spherically bent crystals has many advantages (they have a very high luminosity compared with pinholes and can provide a high spatial resolution over very large fields of view) it presents a disadvantage connected with the necessity to use them, in order to minimize the astigmatism, only for angles of incidence within a few degrees of normal. Such a restriction on the angle of incidence θ, along with the fixed interplanar spacing $(2d)$ of the crystal itself, limits the wavelengths range used now for backlighting diagnostics.

One of the approaches for broadening the spectral range for backlighting diagnostics is to apply torroidally bent crystals, which use different sagittal and meridional radii of curvature in order to eliminate the astigmatism for incident angles far from normal (Vollbrecht *et al.*, 1998; Missalla *et al.*, 1999; Uschmann *et al.*, 2000). However, high-quality torroidal surfaces are more complicated to obtain compared with spherical ones. Another disadvantage of using such crystals for backlighting diagnostics is the very difficult alignment due to constraints on all the six degrees of posi-

Address correspondence and reprint requests to: A. Faenov, MISDC of VNIIFTRI Mendeleevo, Moscow region, 141570, Russia. E-mail: faenov@yahoo.com

tioning freedom. Furthermore, for an ideal torroidal surface and an ideal alignment (see, for more details, a theoretical modeling, which has been done by Uschmann *et al.*, 2000), reasonable spatial resolution in the range of 3–10 μm could be reached only in a field of view around 100 μm, which is not appropriate for current Z-pinch plasma investigations and for the future big scale laser plasma facilities.

Another approach to the broad the range of suitable imaging wavelengths is to increase the variations of produced types of spherically bent crystals and their cuts. Unfortunately not so many types of crystals and their cuts could be bent along a spherical surface with a big enough ratio between the crystal sizes and their radius of curvature.

To avoid the restrictions on using spherically bent crystals with practically any angles of incidence Θ (i.e., to avoid problem with the apparent astigmatism aberrations) Fraenkel *et al.* (1999), Pikuz *et al.* (1999, 2001), Flora *et al.* (2001), and Sanchez del Rio *et al.* (2001) have proposed the modification of traditionally used monochromatic backlighting schemes—the so-called Shadow Monochromatic Backlighting (SMB) scheme or X-ray crystal imaging microscope (XCIM). The traditional X-ray monochromatic backlighting scheme with the spherically bent crystal is shown in Figure 1a. In this scheme the backlighter is placed on the Rowland circle very close to the optical axis of the crystal surface. The object and the detector are mounted at a distances from the crystal according with the usual optical equation

$$1/a + 1/b = 2/R, \tag{1}$$

where R is the crystal radius of curvature, and a and b are the distance from the object to the crystal and from the crystal to the detector, respectively. The magnification of the image is defined by the value $M = b/a$.

The modification of the monochromatic backlighting scheme, the SMB is shown in Figure 1b. A main advantage of the SMB scheme, compared with the usual backlighting scheme, is the possibility to work in a wide range of Bragg angles far from 90°, but still to receive a stigmatic image of the object. In the SMB scheme, the detector is placed at a special fixed position downstream from the crystal between the tangential and sagittal foci. This position depends from on the wavelength (Bragg angle Θ) and the crystal curvature and is defined by the equation (Sanchez del Rio *et al.*, 2001)

$$d = (f_t f_s - f_s^2)/(f_t + f_s), \tag{2}$$

where f_t and f_s are the tangential and sagittal focuses, correspondingly. The magnification in this position is calculated by Sanchez del Rio *et al.* (2001) as $M = d/x$ (see Fig. 1b). To obtain different magnifications in such a scheme it is just simply necessary to move the object along the source–crystal direction (to change distance x) and to keep fixed the backlighter, the crystal, and the detector positions.

In Sanchez del Rio *et al.* (2001) and Pikuz *et al.* (2001) it has been shown experimentally that the SMB scheme allows us to obtain highly spatially resolved ($\sim$5 μm) monochromatic ($\delta\lambda/\lambda \sim 10^{-2}$–$10^{-4}$) images over a large field of view (some square millimeters) for Bragg angles Θ as small as $\sim$40°. A ray-tracing modeling (Sanchez del Rio *et al.*, 2001) confirmed that in such scheme the spatial resolution could be even better than the backlighter source size.

Unfortunately in the SMB scheme, spatial resolution is quite strongly dependent on the source size. Another disadvantage of the SMB scheme, specifically if the crystal has a small enough radius of curvature, is that the object should be placed close enough to the backlighter and it can cause in some cases overheating of the investigated object by the radiation of the backlighter. Such a problem also is typical for the usual backlighting scheme with a Bragg angle close to 90°. Even more often in real experimental conditions the following problem can occur: The object itself screens the beam reflected from the crystal.

In this article we show how to avoid some of the abovementioned problems. In the considered backlighting scheme, the position of the object has been changed and moved downstream of the reflected beam. Experimental results are presented, which were obtained in the case when a test mesh was placed either between the crystal and the tangential focus or after the sagittal focus. The obtained experimental

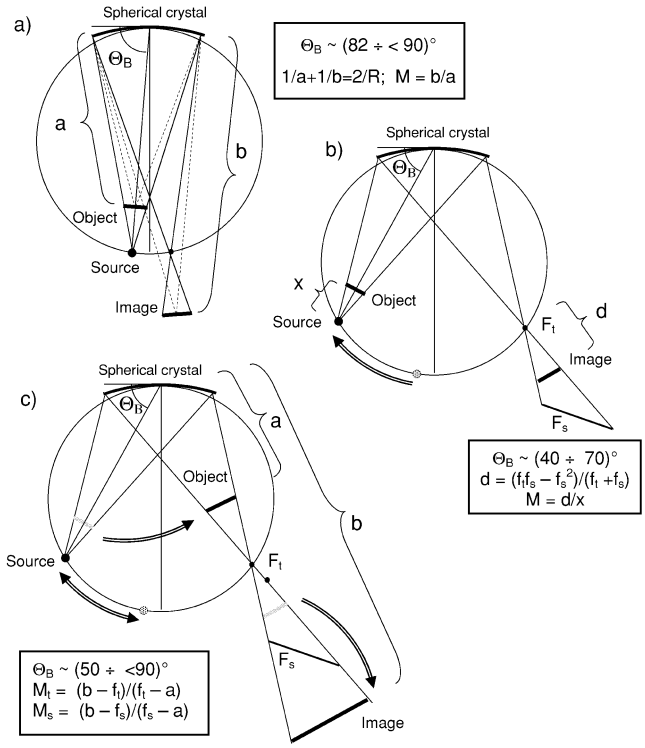

Fig. 1. Evolution of the monochromatic backlighting schemes with spherically bent crystals. a: Traditional scheme, where the distances object–crystal and crystal image are defined by optical equation; b: SMB (or XCIM) scheme, which allows strongly decreased Bragg angle $\ll$90°; c: XMPI scheme proposed in this article with the object placed downstream of the beam reflected from crystal.

results are compared with the results of the ray-tracing calculations, which were performed using the specially developed ray-tracing code ORTO (Labate *et al.*, 2004).

2. X-RAY MONOCHROMATIC PROJECTION IMAGING (XMPI) SCHEME: GENERAL DESCRIPTION AND RAY-TRACING MODELING

As was mentioned above, the described new types of X-ray monochromatic projection imaging (XMPI) schemes are placed somehow between the traditional and the SMB schemes. Such considered schemes are still utilizing the properties of the shadow monochromatization, but for much bigger Bragg angles, which are closer to normal incidence angles (Θ around 50–80° compared with the 20–60°, which is more usual for the SMB scheme, and compared with the 82–87°, which is typical for the traditional backlighting scheme). There are no strong restrictions in the new approaches, which are very important for the SMB scheme, for positions of the backlighting source, the crystal, and the detector. In the SMB scheme, due to such fixed positions, the obtained images are stigmatic. In the new considered XMPI configurations, the positions of the source, the crystal, and the object are flexible, and in such cases the obtained images are astigmatic, but still the information about the space properties of the object are kept with a high enough spatial resolution in both directions.

In XMPI schemes the magnifications are determined by the following equations:

$$M_t = \pm(b - f_t)/(f_t - a) \tag{3}$$

in the tangential direction and

$$M_s = \pm(b - f_s)/(f_s - a) \tag{4}$$

in the sagittal direction.

Here f_t and f_s are the tangential and the sagittal focus, respectively (see eq. (2) and Fig. 1b), a is the distance between the crystal and the object and b is the distance between the crystal and the image (see Fig. 1c).

It is necessary to stress that, due to the big angle of incidence, the reflected beam has an astigmatic structure and the image could be slightly deformed because of the different magnification value in the sagittal and in the tangential directions. In such a case, to reach a geometrical similarity between the image and the object it is sufficient to make a trivial linear geometrical transformation.

2.1. Ray-tracing modeling of the scheme

Ray-tracing simulations of the projection-imaging scheme illustrated above have been performed using the code ORTO (Labate *et al.*, 2004). The geometrical features of different optical setups based on bent Bragg crystals, as well as other optical elements, can be modeled by this code, which is also able to consider the physical characteristics of the interaction with the crystal by taking into account the crystal rocking curve. The code generates, using a Monte Carlo method, a set of rays originating in a given region of the space with a user-defined distribution and propagating toward another region with a suitable angular distribution. The spectral distribution of the source can also be considered (see more details in Labate *et al.*, 2004).

For the simulations described in the present article, a planar source with a Gaussian shape has been used. Each ray thus has its origin on a plane normal to the line joining the source and the center of the crystal (see Fig. 2a) and the probability for this origin to be at distance r from the source center is given by a Gaussian distribution (having its maximum at $r = 0$). A white (uniform) spectrum has been assigned to this source. Because the rocking curve of the crystal has been taken to be uniform in a given angle around the Bragg angle, this means that only the geometrical features of the system have been modeled. Because an almost perfect mica crystal has been used for the experimental tests, this approximation is suitable to provide an estimate of the attainable spatial resolution of the system as well as to study the distortion of the image.

Two different configurations, corresponding to different values of the Bragg angle, have been considered for the following simulations. In both cases, the point X-ray source as well as Gaussian sources, with a FWHM of 15, 30, and 50 μm, were considered. The imaged object was composed of two grids, rotated by 45° to each other, having, respectively, a period of 800 and 60 μm and a wire thickness of 50 and 14 μm. For each simulation, 10^7 rays were sampled, whose direction was uniformly distributed in a solid angle defined by the source position and the four edges of the crystal, whose size was selected as 8×8 mm^2.

Figure 2b,c (left) shows the result of a simulation performed using a Bragg angle $\vartheta_B = 80.5°$ and a crystal with a radius of curvature $R_c = 150$ mm. The detector was considered to be 12×12 mm^2 wide (this corresponds to the whole image in the figure). The source is placed at a distance $c = 148$ mm from the crystal, and the object (position 1 in Fig. 2a) and detector, both oriented normal to the ray coming from the center of the crystal, lie at distances $a = 106$ mm and $b = 410$ mm downstream of the crystal. The corresponding values of the tangential and sagittal magnification of the objects (at the position defined by the ray coming from the center of the crystal) are $M_t \cong 6.25$ and $M_s \cong 5.0$, respectively. A more astigmatic configuration was also considered, using a Bragg angle $\vartheta_B = 67.9°$. The result, using a detector 20×12 mm^2 wide, is shown in Figure 2b,c (right). The distances in the setup were $c = 100$ mm, $a = 62$ mm, and $b = 360$ mm. Since a crystal radius of $R_c = 100$ mm was used, these led to magnifications $M_t \cong 11.25$ and $M_s \cong 4.4$.

From Figures 2b,c it is clearly seen that spatial resolution is good enough for both angles that have been used in the modeling. What is interesting is that even in the case when

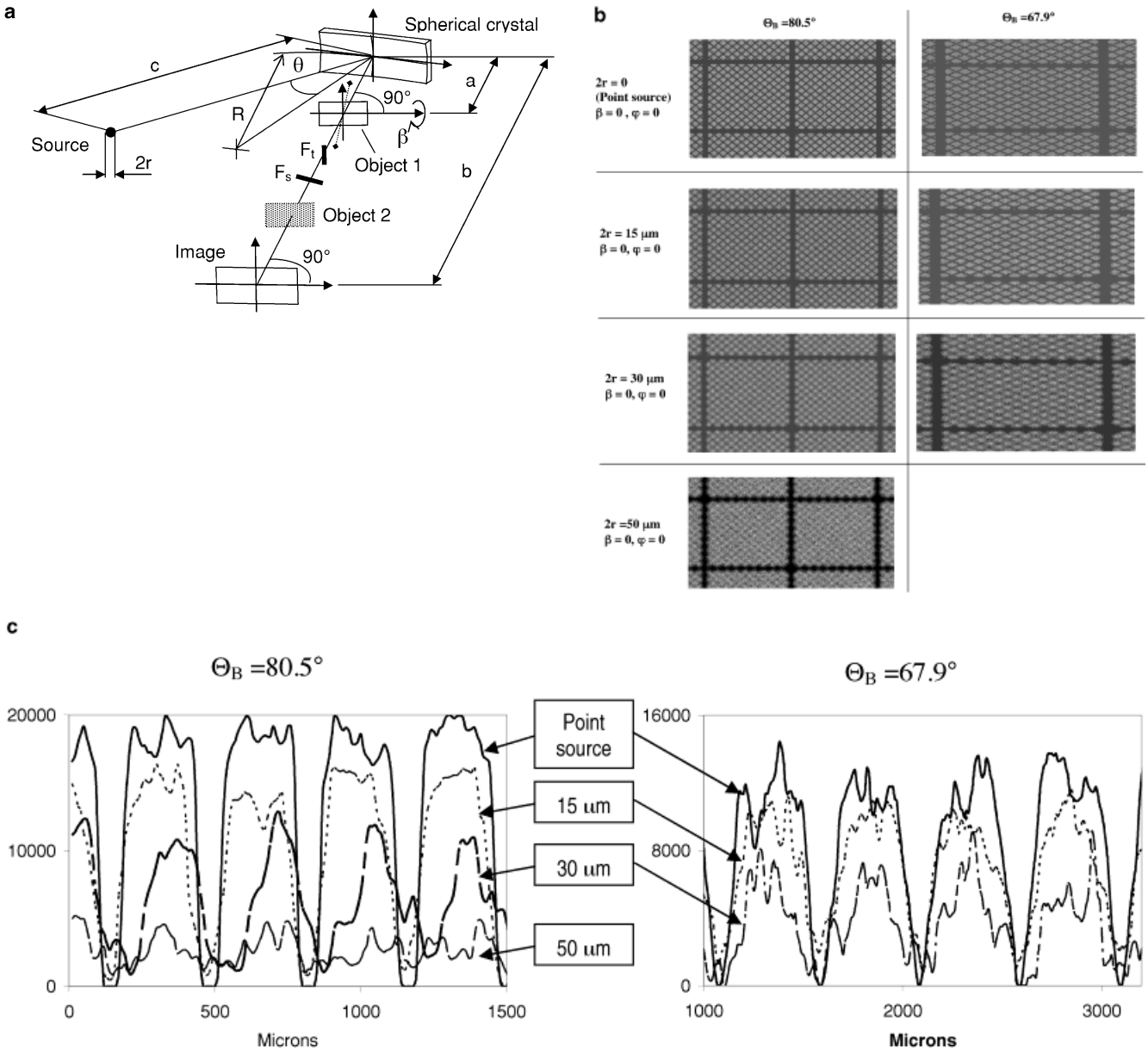

Fig. 2. Ray-tracing modeling of the XMPI scheme with spherically bent crystal in the case when the object (object 1) and detector are placed downstream and perpendicular to the reflected beam. a: Sketch of the scheme used for modeling and experiments; b: simulated images of the double mesh (big mesh has a period 800 μm and wire thickness of 50 μm, small mesh has a period of 60 μm and wire thickness of 14 μm), obtained under Bragg angle 80.5° (left) and 67.9° (right) with different sizes of the source; c: densitograms of the small mesh images for all considered cases.

the size of the backlighting source (30 μm) is two times larger than the size of the object (14 μm) the obtained modeling images clearly resolve the object. This means that even for such a size of the backlighter source a spatial resolution is around 10 μm. The effect of the astigmatism can be clearly seen in the image, but these difficulties could be easily overcome by a simple geometrical transformation without losing spatial resolution of the system.

In some additional modeling the object and the detector were also oriented parallel to the crystal. Figure 3a shows the tilting of the object and the detector to the angle φ. Results of this modeling are presented in Figure 3b,c. It can be clearly seen from this figure that placing the object in such a configuration reduce spatial resolution (compare results presented in Figs. 2b,c (right) and 3b,c). It means that in experiments the object must be oriented as accurately as possible perpendicular to the reflected beam from the center of the crystal.

Finally, to explain a shift of the vertical wires, which was observed in the experimental tests, further simulations were performed with the objects (the meshes) tilted around an axis defined by the plane of the object and the tangential

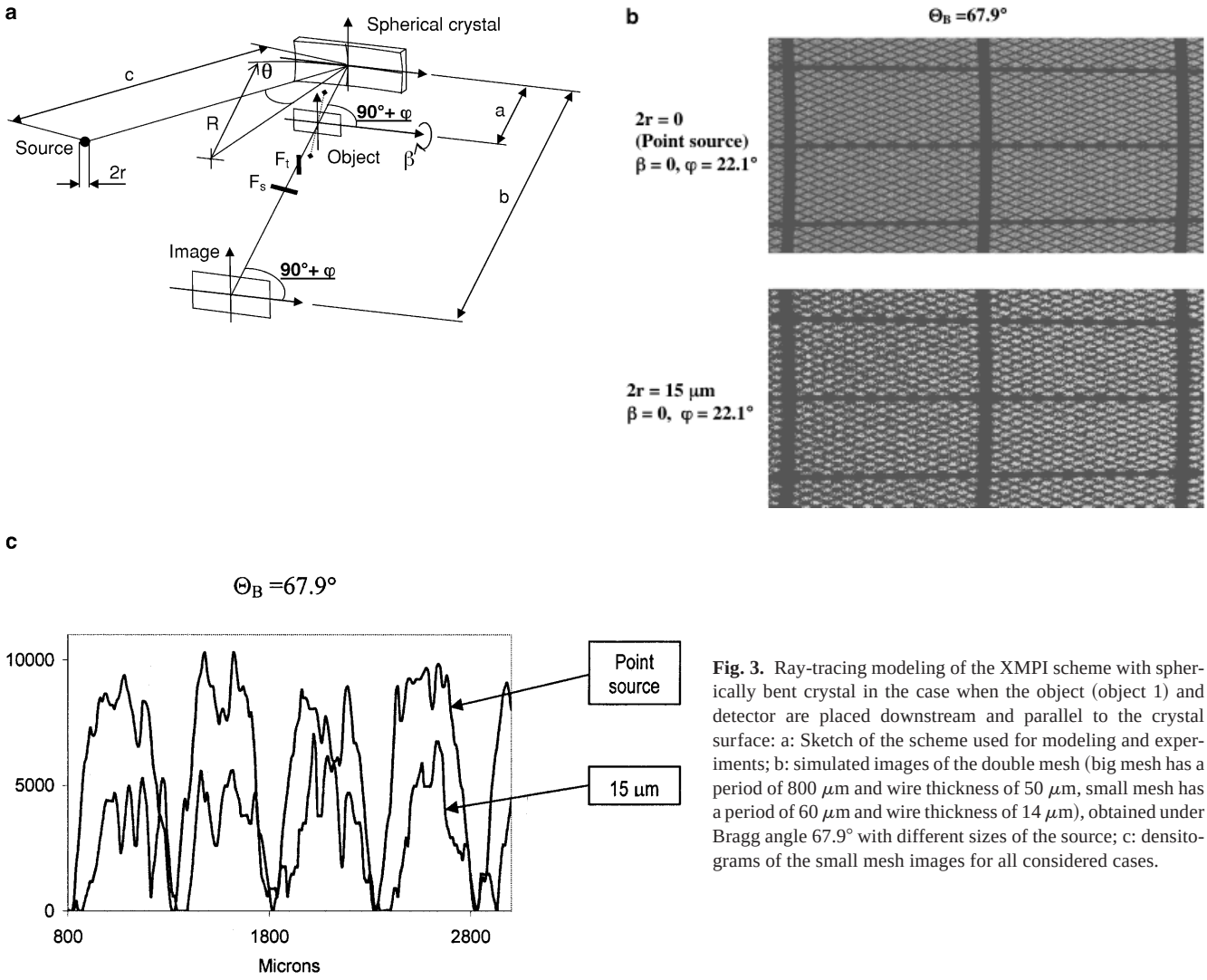

Fig. 3. Ray-tracing modeling of the XMPI scheme with spherically bent crystal in the case when the object (object 1) and detector are placed downstream and parallel to the crystal surface: a: Sketch of the scheme used for modeling and experiments; b: simulated images of the double mesh (big mesh has a period of 800 μm and wire thickness of 50 μm, small mesh has a period of 60 μm and wire thickness of 14 μm), obtained under Bragg angle 67.9° with different sizes of the source; c: densitograms of the small mesh images for all considered cases.

plane of the system. It corresponds that the object was rotated to the angle β (see Fig. 3a). Figure 4 shows the results of a simulation carried out using the same parameters as for the latter one, but now with the object rotated 5° and 20° around this axis (also the source FWHM is in this case 0.0 μm, corresponding to a point source). Figure 4 obviously shows the effect of a misalignment of the object with respect to a perfectly vertical (i.e., normal to the tangential plane) position.

In all the above considered cases, ray-tracing simulations demonstrate very clearly that sharp, well spatially resolved images with an acceptable degree of distortion can be obtained using the scheme illustrated above.

3. EXPERIMENTAL RESULTS AND DISCUSSIONS

Experiments for X-ray monochromatic projection imaging of an object, placed downstream of the reflected beam, were carried out at the "Hercules" laser facility at the "Ente per le Nuove Tecnologie, l'Energia e l'Ambiente" (ENEA) Institute in Frascati, Italy (Bollanti *et al.*, 1996, 1998). This is a XeCl excimer laser with an active volume of $9 \times 4 \times 100$ cm^3 and a wavelength of 0.308 μm. The laser energy was 0.5–1 J, the pulse duration was 12 ns, and the repetition rate was 0.5 Hz. The laser radiation was focused onto a Fe target to form a backlighter source of about 15–25 μm in diameter. Between 500 and 1000 laser shots were needed for obtaining good images on the film. Spherically bent mica crystals, with radius of curvature $R = 100$ mm (working area 8 mm $\times$ 28 mm) and $R = 150$ mm (working area 14 mm $\times$ 48 mm), were used for obtaining monochromatic images.

A couple of meshes (the same parameters as meshes used in ray-tracing modeling), were used as a test object: One mesh was with a period of 800 μm and a diameter of the wires of 50 ± 5 μm and another mesh was with a period of 60 μm and a diameter of the wires of 14 μm. The obtained images were

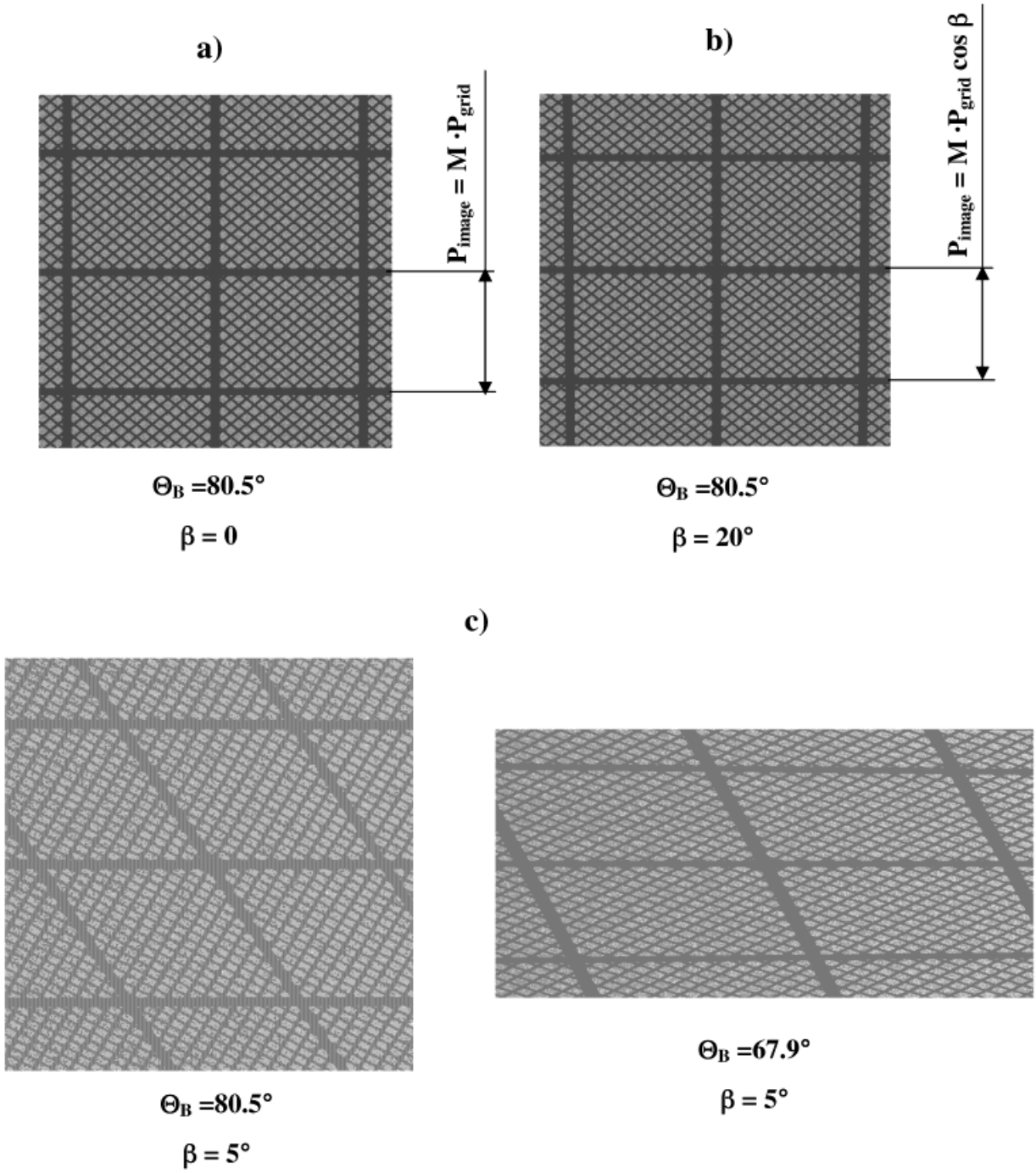

Fig. 4. Ray-tracing modeling results obtained for different positions of meshes and detector. a: The meshes and the detector are perpendicular to the reflected beam; b: the meshes are rotated at the angle β; c: the meshes and the detector are placed parallel to the crystal and after meshes were rotated at angle β.

recorded on Kodak RAR 2492 film. The film holder was protected by a 7-μm Be foil and by two layers of 1-μm polypropylene filters coated with 0.2-μm layers of aluminum. Additional 2-μm polypropylene filters were used to stop the plasma debris from reaching the surface of the crystal.

Three types of experiments have been done. In all such experiments the test object was placed downstream of the reflected beam, at various positions around the tangential and the sagittal focusing points of the beam. The schemes of the setup correspond to the positions of Object 1 and Object 2 in Figures 2a. The numerical parameters of the experimental configurations are presented in the Table 1.

In the first type of experiment (Fig. 2a, object in position 2, and Exp. No. 1 in Table 1), a test mesh was placed after

Table 1. *Parameters of X-ray monochromatic projection imaging (XMPI) schemes used in experiments.*

Exp. No.	Crystal radius of curvature (mm)	Bragg angle (°)	Distance source–crystal p (mm)	Tangential focus q′ (mm)	Sagittal focus q (mm)	Distance crystal–object a (mm)	Distance crystal–image b (mm)
1	150	80.5	148	148	156.4	175	410
2	150	80.5	148	148	156.4	106	410
3	100	67.9	100	86.3	117.3	62	360

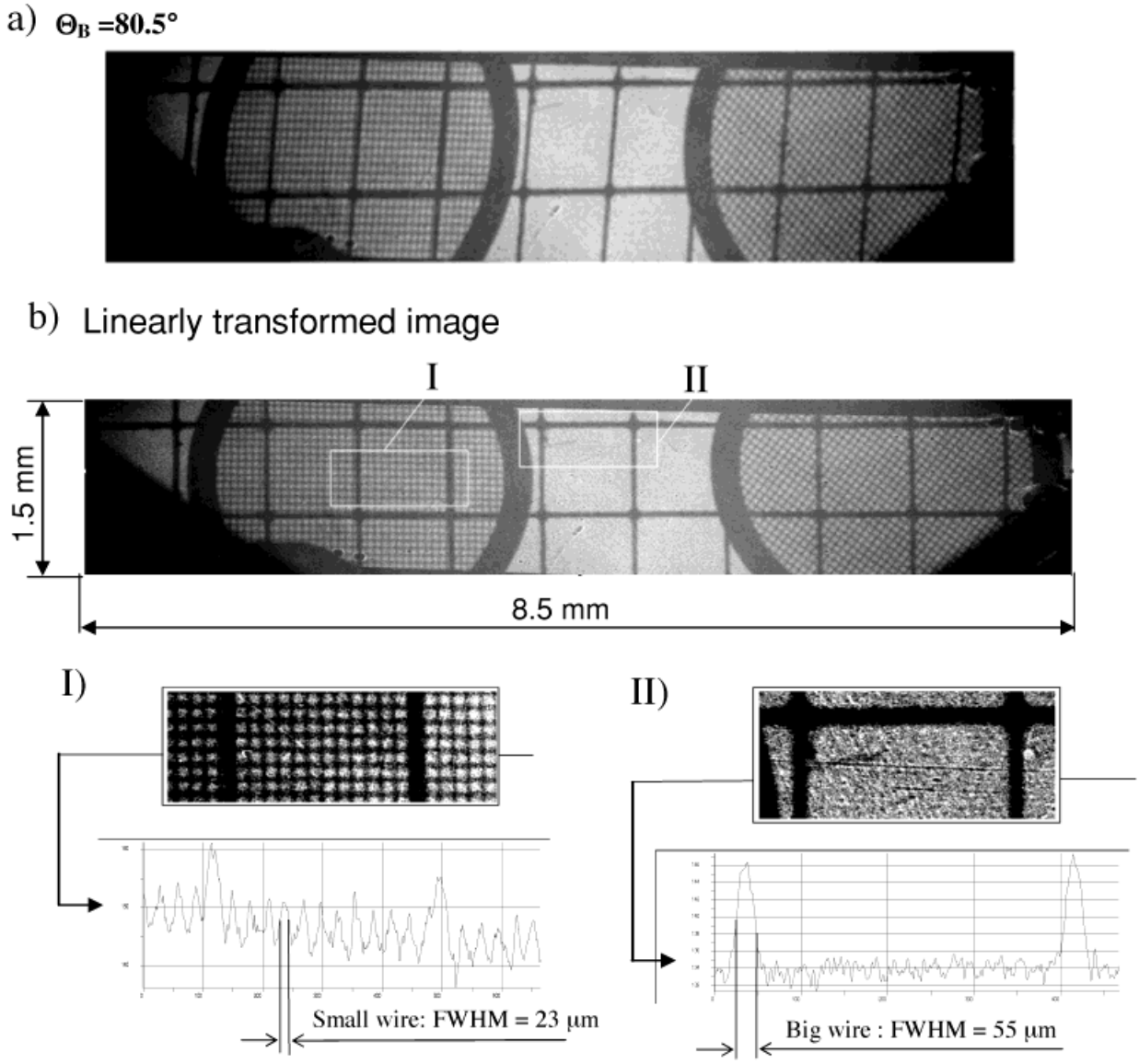

Fig. 5. a: Experimental monochromatic projection image for the double mesh (object 2 position in Fig. 2a), placed downstream of the reflected beam after tangential and sagittal foci (big mesh: period 800 μm; wires 50 ± 5 μm; small mesh: period 60 μm, wires 14 μm), obtained at the wavelength $\lambda = 9.82$ Å (Bragg angle $\Theta = 80.5°$) by mica spherical crystal ($R = 150$ mm) in second order of reflection; b: above image linearly transformed in the case of magnification $M = 9.7^{x}$. Densitograms of the small mesh image are shown in layout (I) and the big mesh image in layout (II).

the tangential and the sagittal foci of the reflected beam. The test mesh contained a big mesh and two small meshes, tilted at 45° to one another. The resulting image obtained in this case, with a good spatial resolution in both the sagittal and the tangential directions, is shown in Figure 5a. Due to the big angle of incidence, the reflected beam has an astigmatic structure and we could see that the image is also slightly deformed because of the different magnification in the sagittal and in the tangential directions for astigmatic beam. In fact in the considered scheme the magnification in the sagittal direction was

$$M_s = -(b - f_s)/(f_s - a) = 13.7^x,$$

whereas in the tangential direction it was

$$M_t = -(b - f_t)/(f_t - a) = 9.7^x.$$

It is necessary to underline that, despite of the astigmatic deformation of the illuminating beam, the image in Figure 5a has a very good spatial resolution in the whole field of view of 8.5×1.5 mm. In such a case, to reach a geometrical similarity between the image and the object it is sufficient to

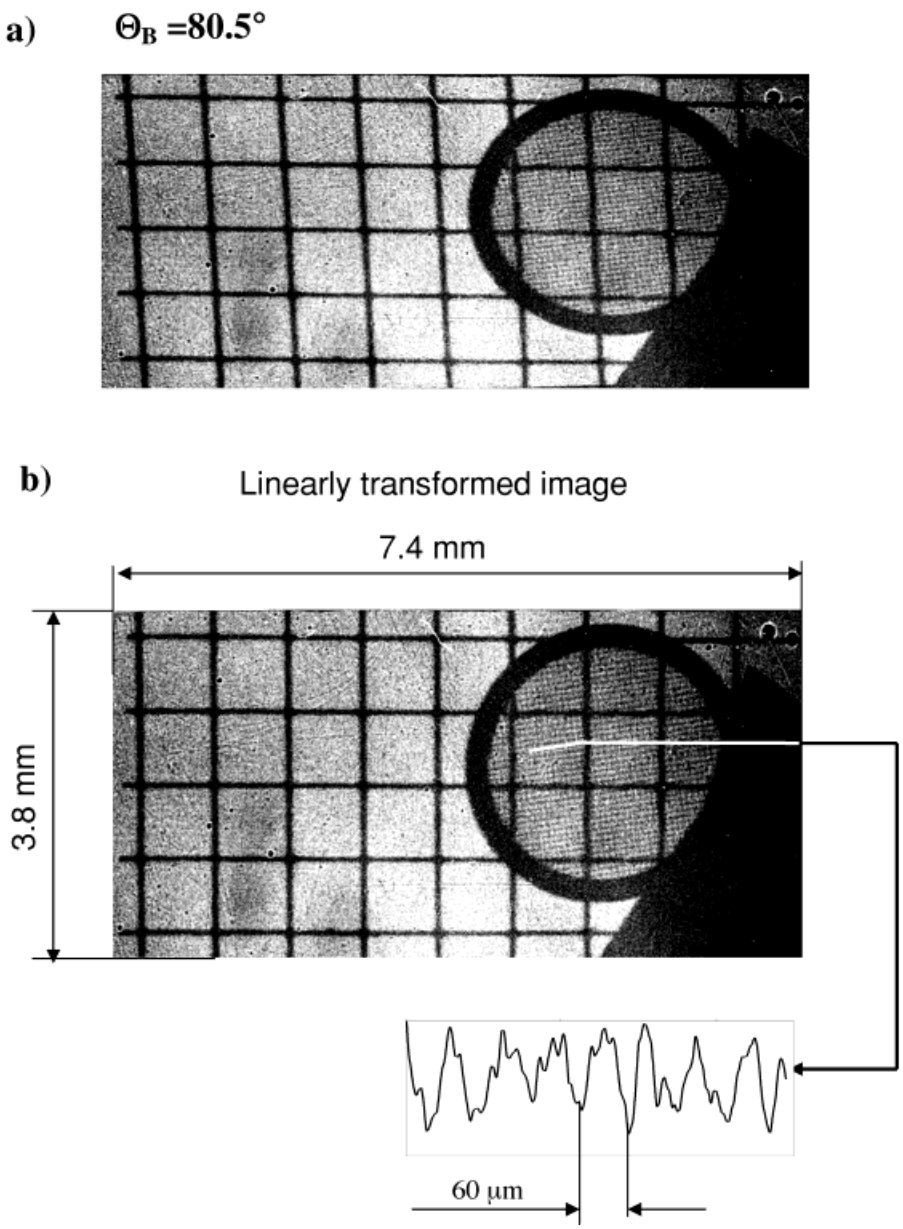

Fig. 6. a: Experimental monochromatic projection image for the double mesh (object 1 position in Fig. 2a), placed downstream of the reflected beam between the crystal and tangential foci (big mesh: period 800 μm, wires 50 ± 5 μm; small mesh: period 60 μm, wires 14 μm), obtained at the wavelength $\lambda = 9.82$ Å (Bragg angle $\Theta = 80.5°$) by mica spherical crystal ($R = 150$ mm) in second order of reflection; b: linearly transformed image. Densitogram of the small mesh image layout shows high spatial resolution.

do a linear geometrical transformation according with the ratio M_s/M_t. The result of this linear transformation is shown in Figure 5b. It is clearly seen that after such a transformation the image is stigmatic, and it has a magnification 9.7^x and a very good correspondence to the initial shape of the object.

For many plasma-backlighting applications it is very important to distinguish the monochromatic backlighting radiation from the strong background radiation of the plasma object. To do it, usually some type of diaphragm is placed at the tangential foci at the Rowland circle. It means that it is very important to consider the backlighting scheme in which the object will stay after the crystal, but inside the Rowland circle, before the tangential foci (the above ray-tracing modeling has been done for this type of scheme). The scheme of such an experiment is presented in Fig. 2a (Object 1 case; see also the description in Table 1, Exp. 2) and the results of this type of experiment is presented in Figure 6a. For a better comparison with the previous experimental scheme, the Bragg angle in this experiment has been chosen the same ($\Theta = 80.5°$) as in the experimental conditions of Figure 5. In experiment 2, which we considered now, the magnification in the sagittal direction was

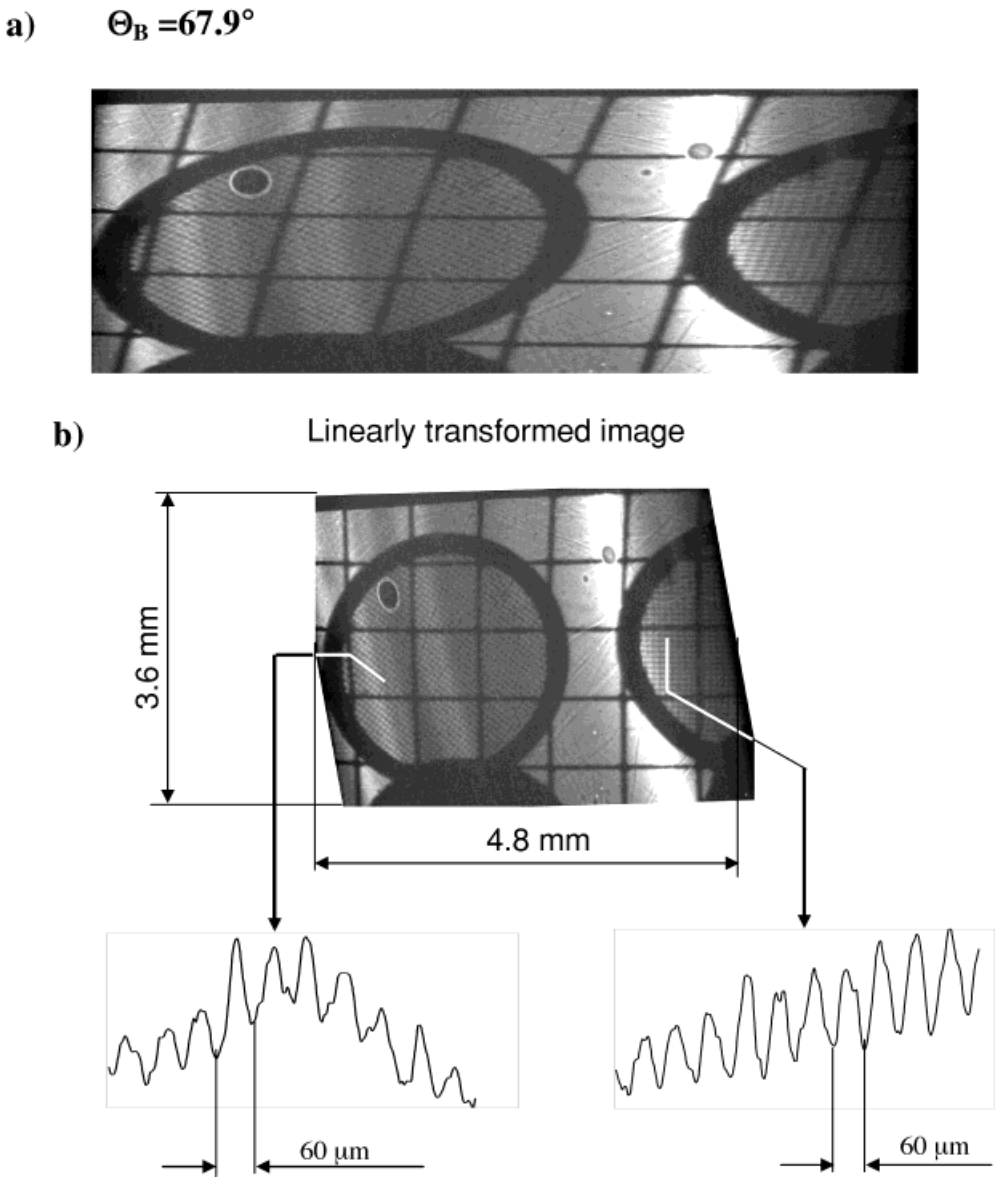

Fig. 7. a: Experimental monochromatic projection image for the double mesh (object 1 position in Fig. 2a), placed downstream of the reflected beam between the crystal and tangential foci (big mesh: period 800 μm, wires 50 ± 5 μm; small mesh: period 60 μm, wires 14 μm), obtained at the wavelength $\lambda = 9.22$ Å (Bragg angle $\Theta = 67.9°$) by spherical mica crystal ($R = 100$ mm) in second order of reflection; b: linearly transformed image. Densitograms of the small mesh image in different directions shows high spatial resolution.

$$M_s = (b - f_s)/(f_s - a) = 5^x$$

whereas in the tangential direction it was

$$M_t = (b - f_t)/(f_t - a) = 6.2^x.$$

We could see that still, despite the astigmatic deformation of the illuminating beam, the image in Figure 6a has a very good spatial resolution in the whole field of view of 7.4 × 3.8 mm^2. Again, like above, to reach the geometrical similarity between the image and the object it is sufficient to do a linear geometrical transformation, according with the ratio M_s/M_t. The result of such a linear transformation is shown in Figure 6b. It is clearly seen that, after such transformation, the image is stigmatic and it has a magnification 5^x and a very good correspondence to the initial shape of the object. From comparison of the images from Figures 2 and 6 we clearly see a very good coincidence between experimental and ray-tracing results.

As was demonstrated by ray-tracing modeling, it is possible to obtain a very good spatial resolution also for bigger Bragg angles. So, in this case it is interesting experimentally to obtain images in such a scheme for bigger Bragg angles, which lay farther from the normal. The result of such an experiment is presented in Figure 7a (see also the description of the experimental conditions in Table 1, Exp. 3). The Bragg angle in this experiment corresponds to ray-tracing modeling and was $\Theta = 67.9°$, so it was very far from the normal. As can be seen from Figure 7a, the astigmatism of the obtained image is very big. But such strong astigmatism does not dramatically decrease the spatial resolution of the image and still in both directions the spatial resolution is very high. In Experiment 3 the magnification in the sagittal direction was

$$M_s = (b - f_s)/(f_s - a) = 5^x$$

whereas in the tangential direction it was

$$M_t = (b - f_t)/(f_t - a) = 12.3^x.$$

Like above, to reach a geometrical similarity between the image and the object it is sufficient to do a simple linear geometrical transformation, according with the ratio M_s/M_t. The result of such a linear transformation is shown in Figure 7b. It is clearly seen that, after such a transformation, the image is stigmatic and it has a magnification 5^x and a very good correspondence to the initial shape of the object.

Thus, from the experiments carried out and from the ray-tracing modeling, it is possible to conclude that when the angles of incidence of the backlighter beams on the crystal were rather big (∼10 and ∼22°), the beams reflected by the crystal always had an astigmatic profile and the obtained images of the objects were astigmatic. Such a disadvantage is crucial in the case of working in the visible spectral range with usual optical devices; but in the case of the X-ray spectral range, where crystal optics have unique properties (due to the Bragg conditions) to reflect only very narrow beams, such a disadvantage is not really essential and it still allows us to obtain images with a sufficiently high spatial resolution in both directions. Furthermore, a simple linear transformation of the images allowed us to reconstruct them with a high enough accuracy (a deformation in all directions not larger than 2% remains for images obtained under an angle of incidence of 10°, and no more then 15% for an angle of incidence of 22°). Due to the small size of the X-ray backlighter source, the reconstructed images have a very high spatial resolution (better than 10 μm for a Bragg angle around 80° and about 15–20 μm for a Bragg angle around 68°) in a big field of view.

4. CONCLUSIONS

In summary, we proposed a new modification of the X-ray backlighting and self-emitting imaging technique (based on the use of spherically bent crystal), which can be efficiently used under Bragg angles far from 90°. The data presented in this article demonstrate that such a technique allows us to obtain X-ray monochromatic backlighting images of investigated objects in a big field of view (some square millimeters), with a spatial resolution up to 10 μm. It gives the possibility to strongly increase the spectral tunability of backlighting imaging systems based on spherically bent crystals, which could be very useful for different plasma diagnostic applications.

REFERENCES

Aglitskiy, Y., Lehechka, T., Deniz, A., Hardgrove, J., Seely, J., Brown, C., Feldman, U., Pawley, C., Gerber, K., Bodner, S., Obenschain, S., Lehmberg, R., McLean, E., Pronko, M., Sethian, J., Stamper, J., Schmitt, A., Sullivan, C., Holland, G. & Laming, M. (1996). X-ray emission from plasmas created by smoothed KrF laser irradiation. *Phys. Plasmas* **3**, 3438–3447.

Aglitskiy, Y., Lehechka, T., Deniz, A. Hardgrove, J., Seely, J., Brown, C., Feldman, U., Pawley, C., Gerber, K., Bodner, S., Obenschain, S., Lehmberg, R., McLean, E., Pronko, M., Sethian, J., Stamper, J., Schmitt, A., Sullivan, C., Holland G. & Laming, M. (1997). X-ray spectroscopy of plasmas created by the Nike KrF laser. *Rev. Sci. Instrum.* **68**, 806–809.

Aglitskiy, Y., Lehechka, T., Obenschain, S., Bodner, S., Pawley, C., Gerber, K., Sethian, J., Brown, C.M., Seely, J., Feldman, U. & Holland, G. (1998). High-resolution monochromatic X-ray imaging system based on spherically bent crystals. *Appl. Opt.* **37**, 5253–5361.

Aglitskiy, Y., Lehechka, T., Obenschain, S., Pawley, C., Brown, C.M. & Seely, J. (1999). X-ray crystal imagers for inertial confinement fusion experiments. *Rev. Sci. Instrum.* **70**, 530–535.

Aglitskiy, Y., Velikovich, A.L., Karasik, M., Serlin, V., Pawely, C.J., Schmitt A.J., Obenschain, S.P., Mostovych,

A.N., Gardner, J.H. & Metzler, N. (2001*a*). Direct observation of mass oscillations due to ablative Richtmyer–Meshkov instability in plastic targets. *Phys. Rev. Lett.* **87**, 265001.

Aglitskiy, Y., Velikovich, A.L., Karasik, M., Serlin, V., Pawely, C.J., Schmitt A.J., Obenschain, S.P., Mostovych, A.N., Gardner, J.H. & Metzler, N. (2001*b*). Direct observation of feedout-related mass oscillations in plastic targets. *Phys. Rev. Lett.* **87**, 265002.

Belyaev, L.M., Gil'varg, A.B., Mikhailov, Yu.A., Pikuz, S.A., Sklizkov, G.V., Faenov, A.Ya. & Fedotov, S.I. (1976). X-ray photography of laser plasmas with the aid of analyzer crystals bent to form second-order surfaces. *Sov. J. Quantum Electron.* **6**, 1121–1122.

Bollanti, S., Cotton, R., Di Lazzaro, P., Flora, F., Letardi, T., Lisi, N., Batani, D., Conti, A., Mauri, A., Palladino, L., Reale, A., Belli, M., Ivanzini, F., Scafati, A., Reale, L., Tabocchini, A., Faenov, A.Ya., Pikuz, T.A. & Osterheld, A. (1996). The development and characterization of an XeCl excimer laser generated soft X-ray plasma source and its applications. *Il Nuovo Cimento* **18D**, 1241–1255.

Bollanti, S., Albertano, P., Belli, M., Di Lazzaro, P., Faenov, A.Ya., Flora, F., Giordano, G., Grilli, A., Ivanzini, F., Kukhlevsky, S.V., Letardi, T., Nottola, A., Palladino, L., Pikuz, T., Reale, A., Reale, L., Scafati, A., Tabocchini, A., Turcu, I.C.E., Vigli-Papadaki, K. & Schina, G. (1998). Soft X-ray plasma source for atmospheric pressure microscopy, radiobiology and other applications. *Il Nuovo Cimento* **20D**, 1685–1701.

Brown, C., Seely, J., Feldman, U., Obenschain, S., Bodner, S., Pawley, C., Gerber, K., Serlin, V., Sethian, J., Aglitskiy, Y., Lehechka, T. & Holland, G. (1997). X-ray imaging of targets irradiated by the Nike KrF laser. *Rev. Sci. Instrum.* **68**, 1099–1102.

Flora, F., Bollanti, S., Lai, A., Di Lazzaro, P., Letardi, T., Grilli, A., Palladino, L., Tomassetti, G., Reale, A., Reale, L., Scafati, A., Bacchetta, L., Alianelli, L., Sanchez del Rio, M., Pikuz, T.A. & Faenov, A.Ya. (2001). A novel portable, high-luminosity monochromatically tuneable X-ray microscope. *Proc. SPIE* **4504**, 240–252.

Fraenkel, M., Zigler, A., Faenov, A.Ya. & Pikuz, T.A. (1999). Large-field high-resolution X-ray monochromatic microscope, based on spherical crystal and high-repetition-rate femtosecond laser-produced plasma. *Physica Scripta* **59**, 246–249.

Hölzer, G., Wehrhan, O., Heinisch, J., Foerster, E., Pikuz, T.A., Faenov, A.Ya., Pikuz, S.A., Romanova, V.M. & Shelkovenko, T.A. (1998). Flat and spherically bent muscovite mica crystals for X-ray spectroscopy. *Physica Scripta* **57**, 301–309.

Koch, J.A., Landen, O.L., Barbee, Jr., T.W., Celliers, P., Da Silva, L.B., Glendinning, S.G., Hammel, B.A., Kalantar, D.H., Brown, C., Seely, J., Bennett, G.R. & Hsing, W. (1998). High-energy X-ray microscopy techniques for laser–fusion plasma research at the National Ignition Facility. *Appl. Opt.* **37**, 1784–1795.

Koch, J.A., Landen, O.L., Hammel, B.A., Brown, C.M., Seely, J. & Aglitskiy, Y. (1999). Recent progress in high-energy, high-resolution X-ray imaging techniques for application to the National Ignition Facility. *Rev. Sci. Instrum.* **70**, 525–529.

Koch, J.A., Aglitskiy, Y., Brown, C., Freeman, R., Hatchett, S., Holland, G., Key, M., MacKinnon, A., Seely, J., Snavely, R., Stephens, R. (2003). 4.5- and 8-keV emission and absorption X-ray imaging using spherically bent quartz 203 and 211 crystals. *Rev. Sci. Instrum.* **74**, 2130.

Labate, L., Galimberti, M., Giulietti, A., Giulietti, D., Gizzi, L.A., Laville, P. & Tomassini, P. (2004). Ray-tracing simulation of an X-ray optics based upon a bent crystal for differential absorption applications. *Laser Part. Beams* **22**, 253–259.

Missalla, T., Uschmann, I., Förster, E., Jenke, G. & von der Linde, D. (1999). Monochromatic focusing of subpicosecond X-ray pulses in the keV range. *Rev. Sci. Instrum.* **70**, 1288–1299.

Pikuz, S.A., Shelkovenko, T.A., Hammer, D.A., Faenov, A.Ya., Pikuz, T.A., Dyakin, A.Ya. & Romanova, V.M. (1995*a*). High luminosity monochromatic X-ray backlighting using an incoherent plasma source to study extremely dense plasmas. *J. Exp. Theor. Phys. Lett.* **61**, 638–644.

Pikuz, T.A., Faenov, A.Ya., Pikuz, S.A., Romanova, V.M. & Shelkovenko, T.A. (1995*b*). Bragg X-ray optics for imaging spectroscopy of plasma microsources. *J. X-ray Sci. Technol.* **5**, 323–340.

Pikuz, S.A., Shelkovenko, T.A., Romanova, V.M., Hammer, D.A., Faenov, A.Ya., Dyakin, V.M. & Pikuz, T.A. (1997). High luminosity monochromatic X-ray backlighting using an incoherent plasma source to study extremely dense plasmas. *Rev. Sci. Instrum.* **68**, 740–744.

Pikuz, T.A., Faenov, A.Ya., Fraenkel, M., Zigler, A., Flora, F., Bollanti, S., Di Lazzaro, P., Letardi, T., Grilli, A., Palladino, L., Tomassetti, G., Reale, A., Reale, L., Limongi, T. & Bonfigli, F. (1999). Large-field high resolution X-ray monochromatic microscope, based on spherical crystal and high-repetition-rate laser-produced plasmas. *Proc. SPIE* **3767**, 67–79.

Pikuz, T.A., Faenov, A.Ya., Fraenkel, M., Zigler, A., Flora, F., Bollanti, S., Di Lazzaro, P., Letardi, T., Grilli, A., Palladino, L., Tomassetti, G., Reale, A., Reale, L., Scafati, A., Limongi, T., Bonfigli, F., Alianelli, L. & Sanchez del Rio, M. (2001). Shadow monochromatic backlighting: Large-field high resolution X-ray shadowgraphy with improved spectral tunability. *Laser Part. Beams* **19**, 285–293.

Sanchez del Rio, M., Faenov, A.Ya., Dyakin, V.M., Pikuz, T.A., Pikuz, S.A., Romanova, V.M. & Shelkovenko, T.A. (1997). Ray-tracing for a monochromatic X-ray backlighting scheme, based on spherically bent crystal. *Physica Scripta* **55**, 735.

Sanchez del Rio, M., Fraenkel, M., Zigler, A., Faenov, A.Ya. & Pikuz, T.A. (1999). Collimation of plasma produced X-rays by spherical crystals: Ray-tracing simulations and experimental results. *Rev. Sci. Instrum.* **70**, 1614–1620.

Sanchez del Rio, M., Alianelli, L., Pikuz, T.A., Faenov A.Ya. (2001). A novel imaging X-ray microscope based on a spherical crystal. *Rev. Sci. Instrum.* **72**, 3291–3303.

Sinars, D.B., Cuneo, M.E., Bennett, G.R., Wenger, D.F., Ruggles, L.E., Vargas, M.F., Porter, J.L., Admas, R.G., Johnson, D.W., Keller, K.L., Rambo, P.K., Rovang, D.C., Seamen, H., Simpson, W.W., Smith, I.C. & Speas, S.C. (2003*a*). Monochromatic X-ray backlighting of wire-array z-pinch plasmas using spherically bent quartz crystals. *Rev. Sci. Instrum.* **74**, 2202–2205.

Sinars, D.B., Bennett, G.R., Wenger, D.F., Cuneo, M.E. & Porter, J.L. (2003*b*). Evaluation of bent-crystal X-ray backlighting and microscopy techniques for the Sandia Z-machine. *Appl. Opt.* **42**, 4059–4071.

Uschmann, I., Fujita, K., Niki, I., Butzbach, R., Nishimura, H., Funakura, J., Nakai, M., Forster, E. & Mima, K. (2000). Time-resolved ten-channel monochromatic imaging of inertial confinement fusion plasmas. *Appl. Opt.* **39**, 5865–5871.

Vollbrecht, M., Treichel, O., Uschmann, I., Gabel, K., Lebert, R. & Forster, E. (1998). Soft-x-ray imaging with torroidally curved thallium acid phthalate crystals in the water window. *Appl. Opt.* **37**, 1803–1807.

Workman, J., Tierney, T., Evans, S., Kyrala, G. & Benage, Jr., J. (1999). One-dimensional X-ray microscope for shock measurements in high-density aluminum plasmas. *Rev. Sci. Instrum.* **70**, 613–616.

Workman, J., Evans, S. & Kyrala, G.A. (2001). One-dimensional X-ray imaging using spherically bent mica crystal at 4.75 keV. *Rev. Sci. Instrum.* **72**, 674–677.